Ray-based Deterministic Channel Modelling for sub-THz Band

Gregory Gougeon, Yoann Corre, Mohammed Zahid Aslam

Ray-based Deterministic Channel Modelling for sub-THz Band

Gregory Gougeon, Yoann Corre, Mohammed Zahid Aslam
{ggougeon, ycorre, zaslam}@siradel.com
SIRADEL
RENNES, FRANCE

***Abstract*— Future wireless communications systems will require large network capacities beyond the capabilities of present and upcoming 5G technology. The trend of considering higher frequencies for their large bandwidths continues today into the sub-THz domain. The BRAVE project considers the frequencies in the 90-200 GHz spectrum, which have been considered in this paper. The challenges of channel modelling at sub-THz frequencies are described along with extensions made to a ray-based deterministic tool. The geographical and physical accuracies inherent to the ray-based tool are exploited to simulate two different scenarios. The first scenario is an indoor office scenario and the second is an outdoor in-street scenario. The application of the updated channel modelling properties of the ray-based tool provides interesting perspectives into the sub-THz channel modelling. This permits the development of realistic models for the evaluation, characterization and eventual deployment of such systems.**

***Keywords*—Sub THz, channel modelling, ray-based model.**

I. INTRODUCTION

The properties of the radio wave propagation in the 90-200 GHz band are not properly known, and no channel model (deterministic or stochastic) has been formally validated and recognized by the scientific community yet. The characteristics of the propagation channel and its modelling are nevertheless critical inputs for several research tasks: definition of adequate scenarios (cell range, supported propagation environments), elaboration of PHY-layer algorithms (e.g. waveform, channel estimation, equalization), evaluation and refinement of multi-antenna systems, link- and system-level simulations.

The scientific propagation community today is producing intensive activity on the mmWave bands that are envisaged for beyond 5G applications. These applications include a wide range of different solutions applied in backhauling, access, indoor and outdoor environments, large bandwidth and high antenna directivity scenarios. Due to the high frequency, very strong obstruction losses exist in these bands. The ITU (International Telecommunications Union) provides details on propagation loss due to attenuation by atmospheric gases, rain, vegetation and penetration (buildings, glass etc.) [1].

Sparse propagation channel is generally observed in mmWave (millimeter-wave) bands, where the line-of-sight (LoS) direct-path is the most dominant component. Many propagation paths that bring significant power at a lower frequency are either attenuated by obstacles or suffer from some interactions' weakness (diffraction, diffuse scattering). That is still true in sub-THz spectrum, and might even be slightly amplified. Nevertheless, some specular strong contributions are still present, leading to a few propagation clusters, along with significant delay and angular spreading. Main contributors are reflections on flat surfaces as walls, floor, or windows. Because the wavelength is lower than 3 mm, small objects in particular metallic objects may also cause a significant echo due to a reflection or scattering. Remark that the channel sparsity is further increased by the use of highly-directive antennas, which will compensate for global higher path-loss at sub-THz frequencies. Some multi-paths transmitted and/or received out of the antennas beamwidth are filtered out. This effect has been captured by [2] where the 60-GHz delay and angular spreads do depend on the antenna beamwidth. Recommendations [2] and [3] propose a beamwidth-dependent model for different scenarios at 28 and 38 GHz in respectively indoor and outdoor environments.

Only few scientific publications report today on channel characterization above 90 GHz. [4] describes and analyses few channel sounding measurements in a shopping mall at 28 and 140 GHz. Similar delay spreads and angular spreads are found in both frequency bands. Paper [5] reports on indoor measurements in bands V (60 GHz), E (70 – 80 GHz) and D (126 – 146 GHz). The delay spread is found to be lower in the D-Band. Even if similar propagation paths can be identified in each band, the longest echoes are not detected in the D-band (possibly due to limitation in the measured power dynamic). Paper [6] presents a large set of measurements in several bands up to 86 GHz with a focus on delay spread also. The conclusion is that delay spread does not vary much with frequency.

Some of these high frequency (up to 100 GHz) properties are available in Geometry-based stochastic

channel models (GBSCM) like WINNER+, METIS, mmMAGIC, MiWEBA or 3GPP. At even higher sub-THz frequencies, channel stationarity and multi-link spatial consistency require complex and accurate modelling of these channels. Ray-based deterministic simulators provide a solution by considering accurate geographical data to provide highly realistic predictions. Indeed, adjustments and calibrations of these models can be realized through measurement campaigns, as and when available.

The various propagation challenges and corresponding channel modelling for sub-THz frequencies is described in Section II. Two different scenarios (indoor and outdoor) are selected and described in Section III and the corresponding results are presented in Section IV. Section V provides some conclusions and perspectives for this ongoing work.

II. Propagation Challenges and Channel Modelling in Sub-THz band

The ray-based engine that is used to create the sub-THz prototype simulator has been successfully employed for more than 15 years in the sub-6 GHz band, and has already been experienced in the past few years in the mmWave domain up to 80 GHz [7]. The main evolutions that have currently been implemented are two-fold:

A. Extension of the EM material properties library up to 200 GHz

The original simulator relies on the definition of materials permittivity and conductivity, in particular those given in [8 – Table 3] for frequencies up to 100 GHz. Based on the limitations of the current knowledge regarding the properties of sub THz spectrum, we decided to simply consider the ITU models at 100 GHz and extend their application up to 200 GHz. These implementations were validated by test simulations that assess the transmission, reflection and diffraction coefficients from the four following materials: glass, concrete, plasterboard and wood. The plasterboard that is almost transparent below 6 GHz leads to more than 20 dB loss over most part of the sub-THz spectrum. Concrete walls are fully opaque above 60 GHz. Outdoor-indoor isolation is thus expected in sub-THz bands as well as room isolation in indoor environment. Also reflection loss is observed constant with frequency while diffraction loss is higher. More precisely, the UTD diffraction loss remains the same at the optical frontiers, but rapidly degrades out of those frontiers. Additional degradation between 2 GHz and 200 GHz is found to be around 20 dB when considering a 90° concrete corner, and incidence angle 45°.

B. Management of highly detailed representation of the environment

The VolcanoURBAN tool [9] predicts the propagation loss above the clutter based on the well-known knife-edge diffraction technique (including some heuristics). 3D multiple paths are created from a ray-launching process: and the way to manage the vegetation obstacles has been improved [10]. Both the transmission through the vegetation and the diffraction on bottom and top of the foliage are considered. The transmission is computed from an average linear loss (dB/m) that is multiplied by the propagation length inside the foliage. This enables far more accurate 3D representation of the trees foliage and street furniture compared to conventional geographical database. Therefore, the prediction of the transmission losses and blockage is made much closer to reality.

The VolcanoURBAN technology has recently been updated to support LiDAR point cloud data. This enables far more accurate predictions by considering detailed actual 3D shapes of individual objects like trees [11].

III. Scenario and Setup

The VolcanoURBAN technology described in Section II has been utilized in an indoor office scenario at sub THz frequencies, details of which are described next.

A. In-office scenario

The considered environment is depicted in Fig. 1; it is a typical single-floor office of size 20 m x 10 m as described in [12]. It is composed of external walls, windows, internal walls, cubicle partitions (2 meters high) and desks. The propagation channel is computed from 10 different access points, which are installed at realistic locations i.e. on the wall or below the ceiling at 2.5 m height. 50 user locations at 1.5 m height are computed; they are distributed in the different rooms of the building. All possible 500 links between the access points and the user locations are predicted, aiming at a statistical overview of the channel properties in this environment.

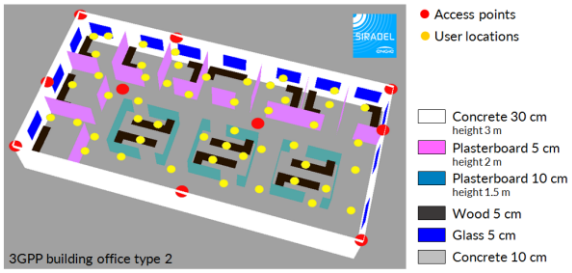

Fig. 1. In-office scenario environment

The access points are considered with either isotropic, 6°-beamwidth or 20°-beamwidth antennas. These three simulations aim at comparing the channel properties as a function of the antenna beamwidth. The 20° and 6°-beamwidth radiation patterns are representative of a beamforming antenna system, which is foreseen to be mandatory in sub-THz communication

in order to focus the energy towards the user, and thus benefit from better gain. In our study, the beam of the access point is automatically oriented towards the best propagation path (either direct or indirect). In all three cases, the transmit power is 0 dBm and the user is equipped with an isotropic antenna. The simulations are performed at frequency from 2 to 200 GHz in order to observe the channel evolution from medium cellular frequency bands to sub-THz bands.

B. In-street scenario

Prediction and characterization of the outdoor sub-THz propagation channel are conducted for urban fixed backhaul links at street level, typically for antennas installed at lamppost height. LiDAR representation and ray-based multi-paths are together exploited to assess the impact of building and vegetation obstructions.

Point cloud LiDAR data that was collected by SIRADEL in the centre of a North-American city (San Jose) is used in this study. The modelled environment is composed of dense buildings with various heights (mostly greater than the simulated antenna heights). Trees are distributed along most of the streets. The study area may be considered as densely vegetated. The street poles, and lampposts in particular, have been precisely classified as shown in Fig. 2.

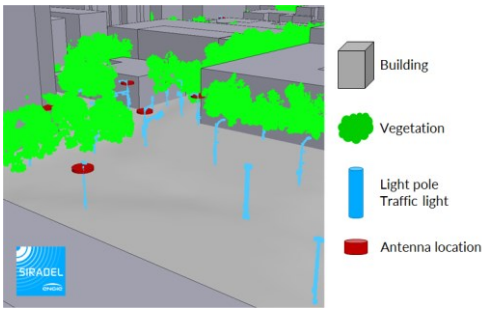

Fig. 2. LiDAR representation

The lampposts are considered as antenna positions and all lamppost-to-lamppost possible links with range lower than 200 meters are computed at frequency 150 GHz. Instead of the traditional LoS/NLoS (non line-of-sight) distinction, the links visibility distinguishes between LoS (no obstruction between the two antennas), NLoS (building obstruction) and NLoS-Vegetation (obstruction by only vegetation). The Excess Path Loss (EPL) is computed for the strongest path, either direct or indirect, assuming that the antennas are highly directive and, therefore, only capture one path. The environment's impact is better highlighted in the EPL prediction compared to the usual path-loss metric. The propagation channel analysis is thus facilitated.

The vegetation linear loss (VLL) has a major impact on all predicted metrics. Three different values are considered, and compared: 6, 9 and 12 dB/m. The reasons are, first, that the vegetation losses vary with the kind of tree, and second, the vegetation impact has not yet been characterized at sub-THz frequencies. Note the simulated losses are far lower than the ones that could have been extrapolated from reference values in [13], but are in agreement with observations made by the authors at mmWave frequencies (tree VLL generally found much below 5 dB/m).

IV. Simulation Results

The channel modelling and characterization for the indoor office and in-street scenarios discussed in Section III are presented next.

A. In-office scenario

The 500 predicted path-loss values are approximated by a traditional model where the median path-loss increases with log of distance:

$$PL = PLI + n \times 20 \log(d) + S \qquad (1)$$

The path-loss PL is expressed in dB; n is the path-loss exponent; the distance d is expressed in meters; the path-loss intersect PLI, in dB, is the median loss at distance 1 meter; S is a shadowing term in dB.

The Path Loss Exponent n is calculated at various frequencies and for all considered antenna beamwidths, as shown in Fig. 3. It is almost constant with frequency in LoS. The 6°-beamwidth antenna is acting as a filter that preserves the dominant direct path but remove most indirect paths, thus n is almost 2. With larger antenna beamwidth, the canyoning effect (or sum of multiple propagation paths caused by the strong reflections in this confined environment) leads to a received power greater or equal to the LoS direct path power; the observed PLE is decreasing down to 1.8. The NLoS path-loss exponent behaves very differently. At lower frequencies, as the transmission losses are weak, the obstructed direct path often remains the dominant path, the NLoS n value is quite similar to the ones observed in LoS situation. But the multi-path effect becomes dominant at higher frequencies, especially above 28 GHz. As the main component in the received power comes from multiple non-obstructed reflected paths, n is rapidly decreasing, and finally reaches values below 1.5 at 150 GHz. Of course, as the NLoS path-loss is growing with frequency, the lower PLE is compensated by a strong increase in the Path Loss Intersect (PLI, i.e. path loss value at distance 1 m). This is shown in Fig. 3 (bottom). The average difference between NLoS PLI at 60 GHz and 150 GHz is 16 dB while it is 8 dB in LoS.

The results allow for a simple implementation of an in-office path-loss model in the sub-THz spectrum, where the LoS probability is given as a function of distance, the median path-loss is calculated from frequency-dependent n and PLI, and the additional shadowing is considered as a lognormal variable with a frequency-dependent standard-deviation (Fig. 4). The graph can be further simplified into approximate formula shown in Table 1, valid in range 90 – 200 GHz.

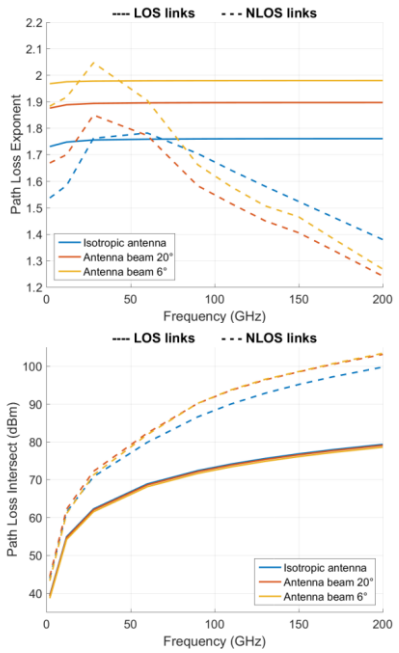

Fig. 3. Path loss exponent (n) and Path loss intersect (PLI)

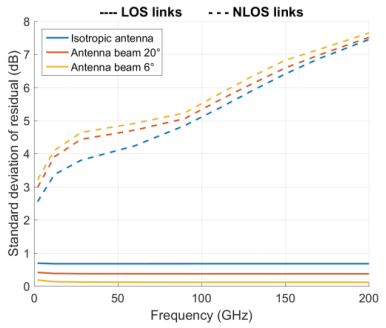

Fig. 4. Standard deviation of the shadowing

Table 1: In-office path-loss model (f is the frequency in GHz)

Acces point antenna	Isotropic	20°-beamwidth	6°-beamwidth
LoS probability (%)		$77 - 1.3 \times d$	
LoS Path-loss exponent PLE	1.76	1.90	1.98
LoS Path-loss intersect (dB)		$33 + 20 \times \log_{10}(f)$	
LoS shadowing std dev (dB)	0.7	0.4	0.1
NLoS Path-loss exponent PLE	$1.97 - 0.0029 \times f$	$1.85 - 0.0030 \times f$	$1.97 - 0.0035 \times f$
NLoS Path-loss intersect (dB)	$33 + 28 \times \log_{10}(f)$	$32 + 30 \times \log_{10}(f)$	$30 + 31 \times \log_{10}(f)$
NLoS shadowing std dev (dB)	$-10 + 3.3 \times \log_{10}(f)$	$-8.9 + 3.1 \times \log_{10}(f)$	$-8.5 + 3.1 \times \log_{10}(f)$

The delay spread and coherence bandwidth are also computed by considering a maximum range of 30 dB in the wideband received power. They are fully characterized by their Cumulative Distribution Functions (CDF) and the median values are plotted as a function of the frequency with distinction between LoS and NLoS.

As discussed in Section III, antennas are equipped with either isotropic, 20° or 6° beamwidths. The effect of this directive (20° or 6°) antenna filtering is observed on the delay spread, which tends to 0 ns with the narrower beam. The LoS delay spread is almost constant with frequency, meaning the major indirect paths remain of same relative magnitude at higher frequencies; they are obviously caused by non-obstructed reflections. The NLoS delay spread versus frequency tends to slowly decrease versus frequency when using a directive antenna, however it is significantly increasing from 2 to 100 GHz with the isotropic access point.

Finally, the coherence bandwidth is larger with the narrowest antenna beams. It is quite constant versus frequency in LoS situation. This can be explained by the strong indirect paths that remain relatively unchanged at higher frequencies for e.g. unobstructed reflections. But the NLoS coherence bandwidth is increasing with frequency, meaning that the weakest indirect paths are filtered out of the 30 dB power range at the highest frequencies, therefore making the channel more flat. As the channel becomes more flat, the coherence bandwidth tends to increase.

A delay spread that increases with frequency does not match with common in-field observations. There are two main reasons. Firstly, the obtained result are specific to the semi-open confined area that has been simulated; secondly, measurements are generally affected by a factor that has not been considered yet, i.e. the receiver sensitivity. In a practical system, some of the individual paths that are distinguished in low frequency bands may be received at a level inferior to the noise floor at a sub-THz frequency. The observed wideband characteristics of the measured channel depend on the receiver sensitivity or maximum allowed path-loss (MAPL) at each considered frequency. Fig. 5 shows how the LoS and NLoS isotopric median delay spreads evolve with frequency, but this time, different MAPL constraints are considered.

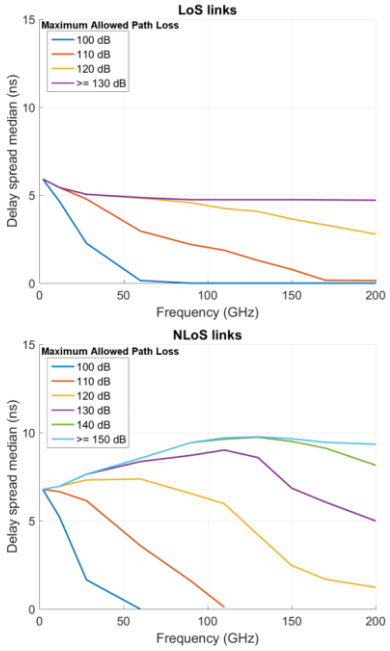

Fig. 5. Median delay spread as a function of the minimum path loss

The conclusion on the delay spread evolution significantly changes depending on the receiver

sensitivity value. The NLoS median delay spread is observed as increasing with frequency when the receiver sensitivity is low, while it rapidly falls to only few ns in mmWave or sub-THz frequencies in case of a limited-performance receiver. The way the wideband channel properties are compared at different frequencies has to be done carefully. The delay spread may be strongly reduced in upper spectrum due to the receiver limitations but not directly to the propagation channel.

The impact of furniture at 150 GHz is studied by addition of shelves, boards, screens and chairs in the same office environment. Some of the links are subject to changes due to more obstructions along the propagation paths, but also due to new scattered paths on furniture as shown in Fig. 6. But globally, as the user terminal is located above many of the added objects (1.5 m), the channel properties in terms of path-loss, delay or angle statistics are not significantly modified.

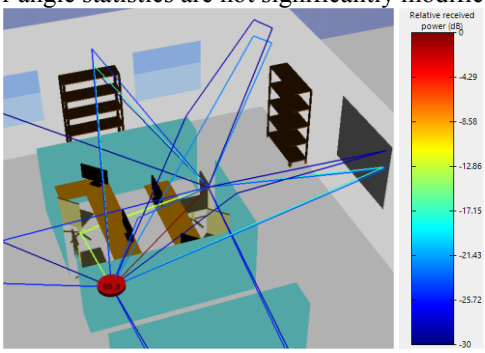

Fig. 6. Propagation paths in office environment with furniture

B. In-street scenario

The distribution between LoS, NLoS and NLoS-Vegetation is shown in Fig. 7 (top) as a function of the distance. At shortest ranges, the poles are mostly in LoS and NLoS-Vegetation situations, then NLoS occurrences rapidly increase, and become the dominant configuration after 85 meters. At this distance, the LoS probability falls below 10 %. The NLoS-Vegetation links are less than 20% at range 200 meters.The CDF of the EPL is plotted in Fig. 7 (bottom) for the three different values of the VLL. The NLoS EPL is about 50 dB higher than non-NLoS. It is hardly impacted by the VLL value, as the dominant propagation path is often due to rooftop diffraction, i.e. occurs above trees. The LoS percentage appears as the left CDF value in the plain curves: about 20%. The highest CDF values are associated to the NLoS-Vegetation situation, where the VLL has a significant impact. As the foliage transmission is combined with foliage diffraction, the distance between EPL curves decreases when the VLL increases, i.e. when diffraction becomes dominant.

Fig. 8 shows the resulting EPL fitting functions for the different VLL values, and the standard deviation of the residual path-loss. This residual path-loss is very high compared to general observations at lower frequencies (standard deviation lower or equal to 10 dB). It globally increases with distance.

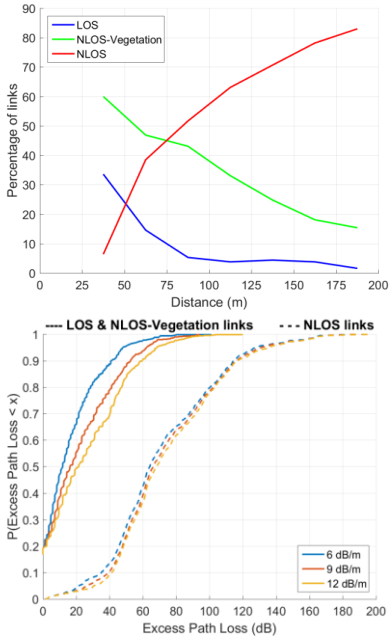

Fig. 7. Distribution of the outdoor propagation results: visibility (left) and Excess Path Loss (right)

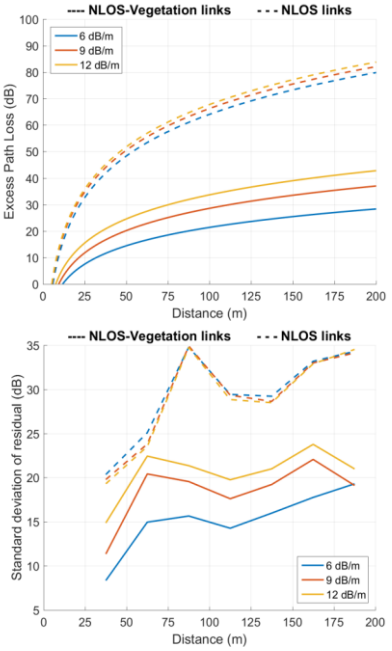

Fig. 8. Excess Path Loss fit and standard deviation of the residual

The highly-directive EPL can be approximated by a lognormal variable, where both the mean value and the standard-deviation are log-distance dependent:

$$\mu\{EPL\} = A + B \times \log(d) \quad (2)$$

$$\sigma\{EPL\} = C + D \times \log(d) \quad (3)$$

The EPL parameters at 150 GHz are given in Table 2 for NLoS and NLoS-Vegetation situations (values are zero in LoS). Those values apply on distances greater

than 25 up to 200 meters. They are proposed as a simplified model for the path-loss experienced in urban street-level sub-THz fixed backhaul.

Table 2: Excess path-loss parameters

	A (dB)		B (dB/dec)		C (dB)		D (dB/dec)	
VLL	NLoS-Veg	NLoS	NLoS-Veg	NLoS	NLoS-Veg	NLoS	NLoS-Veg	NLoS
6 dB/m	-24.8	-40.7	23.1	52.4	-10.2	-6.1	12.7	17.8
9 dB/m	-27.4	-38.7	28.0	52.5	-0.9	-8.2	9.7	18.7
12 dB/m	-26.9	-38.6	30.3	53.2	5.3	-10.1	7.6	19.5

The same simulation model provides coverage maps (received power) as the ones illustrated in Fig. 9, assuming 30 dBm of transmit power. The shadow effect behind trees and buildings can clearly be observed; its impact on the connection range is obvious.

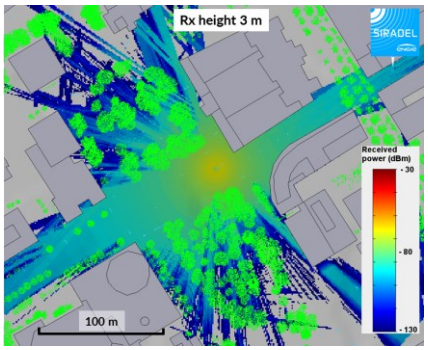

Fig. 9. Coverage from a lamppost transmitter towards a 3-meter high receiver

V. Conclusions and Perspective

The availability of large radio spectrum above 90 GHz offers opportunities to consider networks with immense capacities. Before such networks can be evaluated, it is important to validate the relevant scenarios and their requirements. Such perspective is provided in this paper by considering both indoor and outdoor scenarios at sub-THz frequencies. Definition extensions have been applied to consider adequate physical layer properties to evaluate the channel. Various propagation related properties like excess path loss and delay spread results have been reported for LOS, NLOS with vegetation and NLOS cases. Both isotropic and beamforming antennas have been considered and reported. These initial results correspond to the particular environments considered and further work is required to characterize the sub-THz channel. This on-going work will continue collaborations with the BRAVE project partners to further evaluate and validate the reported scenarios. Further measurements are required to obtain a better understanding of the channel and are expected in the future.

Acknowledgment

The research leading to these results received funding from the French National Research Agency (ANR-17-CE25-0013) within the frame of the project BRAVE.

References

[1] BRAVE, Deliverable D2.0, Propagation channel model and RF impairments definition, Feb. 2019, online: http://www.brave-beyond5g.com/.

[2] ITU-R P.1238-9, Propagation data and prediction methods for the planning of indoor radiocommunication systems and radio local area networks in the frequency range 300 MHz to 100 GHz, Jun. 2017.

[3] ITU-R P.1411-9, Propagation data and prediction methods for the planning of short-range outdoor radiocommunication systems and radio local area networks in the frequency range 300 MHz to 100 GHz, Jun. 2017.

[4] S. Nguyen, J. Jarvelainen, A. Karttunen, K. Haneda and J. Putkonen, "Comparing Radio Propagation Channels Between 28 and 140 GHz Bands in a Shopping Mall", 12th European Conference on Antennas and Propagation (EuCAP), London, UK, Apr. 2018.

[5] L. Pometcu and R. D'Errico, "Characterization of sub-THz and mmWave Propagation Channel for Indoor Scenarios", 12th European Conference on Antennas and Propagation (EuCAP), London, UK, Apr 2018.

[6] S. Nguyen et al., "On the Frequency Dependency of Radio Channel's Delay Spread: Analyses and Findings From mmMAGIC Multi-frequency Channel Sounding", 12th European Conference on Antennas and Propagation (EuCAP), London, UK, Apr 2018.

[7] Y. Corre, T. Tenoux, J. Stéphan, F. Letourneux and Y. Lostanlen, "Analysis of Outdoor Propagation and Multi-Cell Coverage from Ray-Based Simulations in sub-6GHz and mmWave Bands", 10th European Conference on Antennas and Propagation (EuCAP), Davos, Switzerland, Apr 2016.

[8] ITU-R P2040-1, Effects of building materials and structures on radiowave propagation above about 100 MHz, Jul 2015.

[9] Y. Corre and Y. Lostanlen, "Three-dimensional urban EM wave propagation model for radio network planning and optimization over large areas," IEEE Transactions on Vehicular Technology, 2009.

[10] Y. Corre, R. Charbonnier, M. Z. Aslam and Y. Lostanlen, "Assessing the Performance of a 60 GHz Dense Small-Cell Network Deployment from Ray-Based Simulations", IEEE CAMAD 2016, Toronto, Canada, Oct 2016.

[11] J. Stephan, Y. Corre, R. Charbonnier and Y. Lostanlen, "Increased Reliability of Outdoor Millimeter-Wave Link Simulations by Leveraging Lidar Point Cloud", 12th European Conference on Antennas and Propagation (EuCAP), London, UK, Apr 2018.

[12] P. Agyapong, V. Braun, M. Fallgren et al., Simulation guidelines, ICT METIS, Deliverable D6.1, Oct 2013.